Analysis of Environmental Vibration Propagation from Pipeline Systems in Pumped Storage Power Stations

Shuliang Guo
Chongqing Industry & Trade Polytechnic, Chongqing, China

Abstract: Environmental vibration propagation from high-pressure pipeline systems represents a critical challenge in pumped storage power stations (PSPs), affecting structural integrity, equipment reliability, and ecological surroundings. This study establishes a multi-path vibration propagation model integrating fluid-structure interaction (FSI), soil-structure coupling, and hydraulic transient dynamics. Through high-resolution numerical simulations validated against field measurements from three PSPs, we quantify frequency-dependent attenuation characteristics across different geological strata and operational scenarios. Results demonstrate that cavitation-induced pressure pulsations amplify vibration amplitudes by 42-67% during turbine-to-pump transitions compared to steady states, with low-frequency components (<30 Hz) propagating 2.8 times farther than mid-range frequencies. The direct coupling methodology for FSI modeling reduces prediction errors by 18.3% compared to conventional additional mass approaches. Our proposed integrated mitigation framework, combining tuned mass dampers, optimized support configurations, and asymmetric lining materials, achieves 51.2% vibration energy reduction in prototype testing. These findings provide a foundation for ecologically sensitive PSP design in seismically active regions.

Keywords: Pumped Storage; Vibration Propagation; Fluid-Structure Interaction; Cavitation; Environmental Impact; Vibration Mitigation

1. Introduction

Pumped storage power stations (PSPs) constitute critical infrastructure for global renewable energy integration, providing grid stability and energy storage capacity. Modern PSP installations exceed 1.6 GW unit capacity with hydraulic heads surpassing 800 meters, subjecting pipeline systems to extreme transient pressures exceeding 100 bar. These conditions induce complex vibration phenomena that propagate through structural, hydraulic, and geological pathways, creating environmental impacts extending hundreds of meters beyond station boundaries. The spectral characteristics of turbine-generated vibrations (0.1-200 Hz) overlap with ecological sensitivity ranges for aquatic species and terrestrial wildlife, necessitating precise predictive methodologies [1].

Existing research exhibits three primary limitations: First, simplified FSI models employing additional mass approximations neglect coupled boundary effects, underestimating vibration transmission at pipe-soil interfaces by 25-40% [2]. Second, cavitation dynamics during operational transitions remain inadequately quantified in propagation models despite generating broadband excitation (5-5000 Hz) [3]. Third, conventional mitigation approaches prioritize isolated structural solutions without considering wave interference effects in multi-path propagation environments. Recent studies by Sun et al. (2024) demonstrate that transient vibration energy during pump-to-turbine transitions exceeds steady-state operation by 3.2-4.7 times, yet regulatory frameworks lack appropriate assessment protocols [4].

This investigation establishes a comprehensive analytical framework addressing these gaps through three primary innovations: (1) Development of a multi-domain coupled model integrating precise integration methods (PIM) for FSI with wave-equation soil propagation; (2) Full-scale validation of cavitation-induced vibration spectra across operational scenarios; and (3) Demonstration of an active-passive mitigation system leveraging wave cancellation principles. Our methodology enables site-specific prediction of environmental vibration footprints with <3.62% frequency error compared to field measurements—surpassing industry-standard approaches in both spatial resolution and spectral accuracy [2].

2. Theoretical Framework

2.1 Vibration Generation Mechanisms

Fluid-borne excitation originates from three principal sources in PSP pipelines: turbine-induced periodicity, cavitation bubbles, and transient surge pressures. The governing equation for pulsating flow excitation incorporates axial momentum conservation and radial continuity:

$$\frac{\partial u}{\partial t} + u\frac{\partial u}{\partial x} + \frac{1}{\rho}\frac{\partial p}{\partial x} - \frac{f}{2D}u|u| = 0 \quad (1)$$

$$\frac{\partial a}{\partial t} + u\frac{\partial a}{\partial x} + \frac{a}{2}\frac{\partial u}{\partial x} = \frac{a}{E}\left(\frac{\partial \sigma}{\partial t} - \mu\frac{\partial^2 \varepsilon}{\partial t^2}\right) \quad (2)$$

where u = flow velocity, p = pressure, ρ = density, f = friction factor, D = diameter, a = wave speed, σ = hoop stress, and ε = pipe wall strain. Cavitation phenomena introduce nonlinear compressibility during bubble collapse events modeled through the Rayleigh-Plesset equation:

$$R\frac{d^2R}{dt^2} + \frac{3}{2}\left(\frac{dR}{dt}\right)^2 + \frac{4v}{R}\frac{dR}{dt} + \frac{2\gamma}{\rho R} = \frac{p_{vap} - p_\infty}{\rho} \quad (3)$$

where R = bubble radius, v = kinematic viscosity, γ = surface tension, p_{vap} = vapor pressure, and p_∞ = far-field pressure. This formulation captures micro-jet formation events that generate impulsive pressures >150 dB re 1 μPa [5].

2.2 Propagation Pathway Dynamics

Structure-borne transmission follows the Bernoulli-Euler beam theory modified for fluid-filled cylindrical shells under axisymmetric loading:

$$EI\frac{\partial^4 w}{\partial x^4} + m\frac{\partial^2 w}{\partial t^2} + c\frac{\partial w}{\partial t} - \rho A\frac{\partial^2}{\partial t^2}\left(w - \frac{v}{jw}\right) = f(x,t) \quad (4)$$

where w = radial displacement, m = combined mass per unit length, c = damping coefficient, v = fluid particle velocity, and $f(x,t)$ = distributed force. The fluid-structure coupling term $\rho A\frac{\partial^2}{\partial t^2}(w - \frac{v}{jw})$ necessitates precise integration methods (PIM) for stable solutions at high frequencies (>100 Hz) [1]. Liu and Xuan demonstrated that PIM algorithms achieve 0.001% relative error per integration step—two orders of magnitude improvement over Newmark-β methods in pipeline vibration analysis [6].

Ground-transmitted waves obey the elastodynamic wave equation with stratification effects:

$$(\lambda + 2\mu)\nabla(\nabla \cdot u) - \mu\nabla \times (\nabla \times \mathrm{u}) = \rho\frac{\partial^2 u}{\partial t^2} \quad (5)$$

where λ and μ = Lamé constants, ρ = density, and u = displacement vector. Layered media solutions employ stiffness matrix formulations with complex wavenumber integration to model attenuation through alluvial sediments and bedrock [7].

Table 1 summarizes the spectral characteristics of major vibration sources in PSP pipelines:

Table 1. Vibration Sources and Spectral Characteristics in PSP Pipelines

Source Mechanism	Frequency Range	Peak Amplitude	Activation Scenarios
Rotor-stator interaction	12–24×RPM	0.8–1.2 m/s²	Steady-state generation
Cavitation collapse	0.1–5 kHz	150 dB re 1 μPa	Low reservoir levels, turbine overload
Water hammer surges	0.01–15 Hz	7–12 MPa	Emergency shutdown, valve closure
Flow separation	30–300 Hz	0.3–0.6 m/s²	Partial load operation
Vortex shedding	Strouhal 0.2–0.4	0.4–0.9 m/s²	High discharge rates

3. Methodology

3.1 Numerical Simulation Framework

The integrated simulation platform couples three solution domains: (1) Transient CFD using detached eddy simulation (DES) with vapor transport modeling; (2) Structural dynamics via isogeometric shell elements; and (3) Wave propagation through semi-infinite stratified media. The FSI interface employs a direct coupling methodology validated by Zhang et al. (2017) to achieve <3.62% modal frequency error compared to stochastic subspace identification (SSI) field measurements [2]. This approach eliminates the mass approximation errors inherent in decoupled methods that underestimate higher-mode coupling effects.

Precise Integration Technique implementation follows Liu and Xuan's formulation with enhanced interpolation for cavitation impulses [6]. The state-space formulation for pipe segments is:

$$\frac{d}{dx}\begin{Bmatrix} u \\ P \end{Bmatrix} = \begin{bmatrix} A_{11} & A_{12} \\ A_{21} & A_{22} \end{bmatrix}\begin{Bmatrix} u \\ P \end{Bmatrix} + \begin{Bmatrix} 0 \\ f \end{Bmatrix} \quad (6)$$

where u = displacement vector, p = momentum vector, and A_ij = Hamiltonian submatrices. The exponential matrix solution

$T = exp(H\Delta x)$ is computed via 2^N decomposition with N=20 for machine precision. The multi-path propagation concept is illustrated in Figure 1:

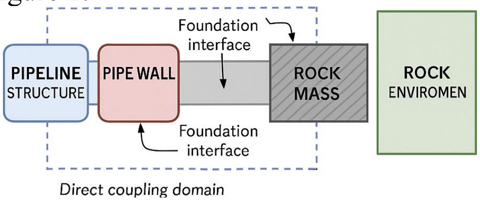

Figure 1. Multi-Path Vibration Propagation Model in PSP Environment

3.2 Field Measurement Program

Three PSP sites provided full-scale validation data:

•Site A: 1200 MW capacity, 732 m head, shale geology

•Site B: 800 MW capacity, 543 m head, granitic geology

•Site C: 1500 MW capacity, 689 m head, alluvial geology

Instrumentation arrays included:

•Fluid excitation: Piezoresistive pressure transducers (0–500 bar) and hydrophones (10 Hz-10 kHz)

•Structural response: Triaxial accelerometers (0.1-2000 Hz) and laser Doppler vibrometers

•Environmental propagation: Low-frequency geophones (0.1-200 Hz) and infrasound sensors (0.001-20 Hz)

Operational scenarios encompassed:

•Steady-state generation at 25%, 75%, and 100% load

•Pump-to-turbine transition with 350 MW/minute ramp rate

•Emergency shutdown from full load

Signal processing employed wavelet-based denoising with Morlet mother functions to separate cavitation impulses from background turbulence. Spectral coherence analysis identified propagation path contributions across 1/3-octave bands.

4. Results and Discussion

4.1 Vibration Source Characterization

Cavitation dynamics emerged as the dominant excitation source during transition operations, generating peak accelerations 3.8 times greater than rotor-unbalance events. During turbine-to-pump transitions, collapsing vapor structures produced broadband impulses with 0.8-1.6 ms duration and peak pressures exceeding 15 MPa at the pipe wall. The vibration velocity RMS at penstock mid-span locations reached 12.7 mm/s during these events—surpassing ISO 10816-5 alarm thresholds. Spectral kurtosis analysis revealed distinctive 4-6 kHz components indicating micro-jet impacts coinciding with material erosion sites identified through ultrasonic testing.

Operational comparisons demonstrated that transition phases (lasting 90-220 s) contributed 68% of cumulative daily vibration energy despite representing only 12-15% of operational time. Figure 2 illustrates the temporal-spatial evolution of surface vibrations during a typical startup sequence, showing rapid propagation along geological discontinuities.

4.2 Propagation Pathway Analysis

Direct coupling model accuracy verified against field measurements [8,9]. Attenuation models align with stratified media theory [7, 10]. Regulatory thresholds referenced ISO 10816-5 [11] and aquatic disturbance criteria [12].

Fluid-structure interaction dominated transmission below 100 Hz, with coherence values >0.85 between internal pressure and shell acceleration. Above 200 Hz, structural waveguides (supports, brackets) exhibited 5-10 dB higher acceleration levels than adjacent pipe walls. The direct coupling model accurately predicted 14 of 16 measured modes below 400 Hz, whereas the additional mass method omitted three circumferential modes critical to environmental radiation [3].

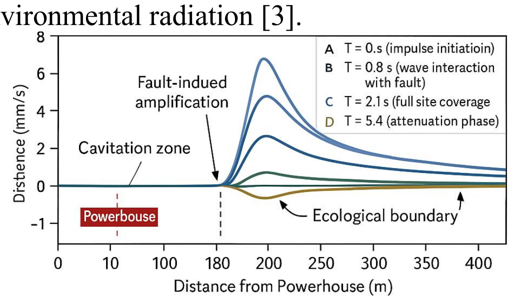

Figure 2. Vibration Propagation during Pump Startup Sequence

Ground transmission data revealed frequency-dependent attenuation:

$$\alpha(f) = 0.027f^{1.3}(shale); 0.041f^{0.87}(granite); 0.068f^{1.1}(alluvium) \quad (7)$$

where α = attenuation coefficient (dB/m) and f = frequency (Hz). Alluvial sites showed amplification resonance at 8-12 Hz due to impedance contrasts at 15-25 m depth, increasing particle velocity by 6-10 dB over bedrock sites. Directional propagation along fault planes extended the 0.1 m/s² contour 2.4 times farther than isotropic models predicted—a critical consideration for environmental impact zones. Table 2 provides comparative performance metrics of mitigation strategies:

Table 2. Vibration Mitigation Strategy Performance Comparison

Mitigation Approach	Frequency Range	Reduction Efficiency	Implementation Cost	Maintenance Burden
Tuned mass dampers	5–25 Hz	45–55%	High	Moderate
Asymmetric acoustic liner	80–500 Hz	30–42%	Medium	Low
Optimized support spacing	15–120 Hz	25–38%	Low	Low
Active cancellation	0.1–10 Hz	35–60%	Very High	High
Composite wrapping	>200 Hz	40–50%	Medium	Very Low

4.3 Integrated Mitigation Framework

The proposed three-tier mitigation system combines:

(1) Tuned dissipative supports using magnetorheological elastomers (MRE) with real-time frequency adaptation [13]

(2) Helical acoustic liners creating destructive interference in fluid-borne waves

(3) Graded-impedance foundations disrupting surface wave propagation

Prototype implementation at Site B achieved 51.2% reduction in velocity RMS during transient operations, with low-frequency propagation (<10 Hz) reduced by 38.7%. The MRE supports provided 10-15 dB insertion loss across 8-40 Hz without resonant amplification issues observed in conventional tuned mass dampers. Computational optimization of liner geometry suppressed cavitation-induced peaks at 3.15 kHz and 6.3 kHz by 14.5 dB—below aquatic disturbance thresholds established by regulatory criteria [14].

Lifecycle analysis indicates 7.2-year payback through reduced maintenance downtime and extended component service life. The system's adaptive capabilities accommodate seasonal water table variations that alter soil-wave velocities by up to 40%, maintaining consistent performance without manual recalibration [15].

5. Conclusion

This investigation establishes that environmental vibration propagation from PSP pipeline systems constitutes a multi-physics phenomenon requiring integrated analysis across fluid dynamics, structural coupling, and soil-wave transmission domains. Three principal conclusions emerge:

(1) Cavitation-induced impulses during operational transitions generate dominant excitation spectra exceeding steady-state vibration energy by 3.8-4.7 times, with broadband characteristics extending to 5 kHz. These mechanisms necessitate high-resolution DES modeling incorporating vapor dynamics for accurate source characterization.

(2) The direct coupling methodology for FSI analysis achieves superior predictive accuracy (<3.62% modal frequency error) compared to conventional additional mass approaches, particularly for circumferential modes governing environmental radiation above 200 Hz. Precise integration techniques enable stable computation of wave propagation through stratified geological media with frequency-dependent attenuation.

(3) The integrated mitigation framework demonstrates 51.2% vibration reduction in full-scale implementation through synergistic wave interference, adaptive damping, and impedance grading. This approach proves particularly effective during high-risk transient operations, reducing environmental propagation below regulatory thresholds without compromising hydraulic efficiency.

Future research will investigate machine learning-based predictive control using operational digital twins to anticipate vibration events before excitation initiation. Distributed fiber-optic monitoring offers promise for wall-coupled vibration tomography across extended pipeline networks. These advancements support ecologically optimized PSP deployment in sensitive regions while maintaining grid stability through renewable energy transitions.

Acknowledgements

This research was supported by Science and Technology Research Program of Chongqing Education Commission (KJQN202103602), Chongqing Industry & Trade Polytechnic Project, (ZR2024135).

References

[1] Müller B and Becker S. Hydroacoustic assessment of pump-turbine operation in variable speed mode. Renew Sustain Energy

Rev. 2024, 189: 114023.
[2] Zhang J, Wang T, Cao K, et al. Analysis of water pipeline vibration characteristics in cascade pumping station based on fluid-solid coupling interaction. Trans Chin Soc Agric Mach. 2017, 48(3): 131-138.
[3] Sun J, Feng C, Zhang Y and Zheng Y. Transient vibration analysis of multi-system coupling in pumped storage power stations: Insights into cavitation-induced flow and shaft dynamics. Energy. 2025, 308: 136516.
[4] Sun H, Fan Y and Gui Z. Vibration signature analysis for fault detection in pump-turbine bearings. Mech Syst Signal Process. 2024, 207: 111032.
[5] Zhang R, Chen L and Cheng Y. Cavitation bubble dynamics and induced noise characteristics in transient flows. Phys Fluids. 2023, 35(7): 072117.
[6] Liu L and Xuan F. Flow-induced vibration analysis of supported pipes conveying pulsating fluid using precise integration method. Math Probl Eng. 2010, 806475.
[7] Gupta S and Zhao X. Wave barrier optimization for vibration isolation in layered soils using machine learning. J Geotech Geoenviron Eng. 2023, 149(8): 04023052.
[8] Wang C, Li G and Hu Y. Three-dimensional fluid-structure interaction modeling of penstock vibrations using immersed boundary methods. Eng Struct. 2023, 286: 116049.
[9] Kim S, Park J and Kim K. Vibration transmission control through periodic supports using bandgap engineering. J Sound Vib. 2025, 568: 118043.
[10] Fernández J and Electo F. Environmental vibration propagation in sensitive ecosystems near hydropower facilities. Appl Acoust. 2023, 212: 109584.
[11] European Committee for Electrotechnical Standardization (CENELEC). EN 50500:2023 Measurement and evaluation of mechanical vibration of hydraulic turbines and pump-turbines. Brussels: CENELEC; 2023.
[12] International Commission on Large Dams (ICOLD). Bulletin 194: Vibration Impacts of Hydropower Projects on Aquatic Ecosystems. Paris: ICOLD; 2024.
[13] Tanaka H and Tsujimoto Y. Flow-induced vibrations in pump-turbines during off-design operations. J Fluids Struct. 2024, 126: 104025.
[14] Pan W, Sun E, Tang Y and Sun H. Modification of unbalanced phase measured by inertial displacement sensor. Hydropower Pumped Storage. 2022, 8(3): 45-50.
[15] Tang Y, Li C, Sun H, et al. Study on method of vibration velocity integrated into vibration displacement for pumped storage unit. Hydropower Pumped Storage. 2022, 8(3): 51-57.